Energy Flux Densities near the Electron Dissipation Region in Asymmetric Magnetopause Reconnection

J. P. Eastwood,[1,*] M. V. Goldman,[2] T. D. Phan,[3] J. E. Stawarz,[1] P. A. Cassak,[4] J. F. Drake,[5] D. Newman,[2] B. Lavraud,[6,7] M. A. Shay,[8] R. E. Ergun,[9] J. L. Burch,[10] D. J. Gershman,[11] B. L. Giles,[11] P. A. Lindqvist,[12] R. B. Torbert,[13,10] R. J. Strangeway,[14] and C. T. Russell[14]

[1]*The Blackett Laboratory, Imperial College London, London SW7 2AZ, United Kingdom*
[2]*Department of Physics, University of Colorado, Boulder, Colorado 80303, USA*
[3]*Space Sciences Laboratory, University of California, Berkeley, California 94720, USA*
[4]*Department of Physics and Astronomy and Center for KINETIC Plasma Physics, West Virginia University, Morgantown, West Virginia 26506, USA*
[5]*Department of Physics/Institute for Physical Science and Technology, University of Maryland, College Park, Maryland 20742, USA*
[6]*Laboratoire d'Astrophysique de Bordeaux, Univ. Bordeaux, CNRS, B18N, allée Geoffroy Saint-Hilaire, 33615 Pessac, France*
[7]*Institut de Recherche en Astrophysique et Planétologie, CNRS, CNES, Université de Toulouse, 31028 Toulouse Cedex 4, France*
[8]*Department of Physics and Astronomy, University of Delaware, Newark, Delaware 19716, USA*
[9]*LASP/Department of Astrophysical and Planetary Sciences, University of Colorado, Boulder, Colorado 80303, USA*
[10]*Southwest Research Institute, San Antonio, Texas 78238, USA*
[11]*NASA, Goddard Space Flight Center, Greenbelt, Maryland 20771, USA*
[12]*KTH Royal Institute of Technology, SE-100 44 Stockholm, Sweden*
[13]*University of New Hampshire, Durham, New Hampshire 03824, USA*
[14]*Institute of Geophysics, Earth, Planetary, and Space Sciences, University of California, Los Angeles, Los Angeles, California 90095, USA*

(Received 30 December 2019; revised 29 October 2020; accepted 24 November 2020; published 30 December 2020)

Magnetic reconnection is of fundamental importance to plasmas because of its role in releasing and repartitioning stored magnetic energy. Previous results suggest that this energy is predominantly released as ion enthalpy flux along the reconnection outflow. Using Magnetospheric Multiscale data we find the existence of very significant electron energy flux densities in the vicinity of the magnetopause electron dissipation region, orthogonal to the ion energy outflow. These may significantly impact models of electron transport, wave generation, and particle acceleration.

DOI: 10.1103/PhysRevLett.125.265102

Introduction.—Magnetic reconnection is of particular importance to astrophysical, solar, space, and laboratory plasmas because it rapidly releases energy stored in the magnetic field surrounding current sheets, converting it into particle acceleration and heating [1–4]. A key issue in all contexts is energy partition, particularly where observations are incomplete [5–7]. At a general level we can write

$$\frac{\partial}{\partial t}(U_e + U_i + U_{\mathrm{EM}}) + \nabla \cdot (\boldsymbol{Q}_e + \boldsymbol{Q}_i + \boldsymbol{S}) = 0,$$

where $U_{e,i}$ and $\boldsymbol{Q}_{e,i}$ are the electron and ion total (bulk flow + thermal) energy densities (in units of joules per meter cubed) and energy flux densities (in units of watts per meter squared). U_{EM} is the electromagnetic energy density, and $\boldsymbol{S}$ is the Poynting flux density, e.g., [8,9]. In certain discipline-specific literature, for convenience the $\boldsymbol{Q}_{e,i}$, and indeed $\boldsymbol{S}$, are often referred to in a shorthand way as "energy fluxes" while in reality it should be emphasized that they are vectors and not the scalar energy fluxes resulting from integration of the (vector) flux density over a surface. Ultimately energy transport through the whole system is a function of the energy flux, so giving importance to the sizes of the regions where the energy flux density is present.

A common approach (the "standard decomposition") is to express the energy flux density of species s, $\boldsymbol{Q}_s$, as the sum of the kinetic energy flux density, $\boldsymbol{K}_s$, enthalpy flux density, $\boldsymbol{H}_s$, and heat flux density, $\boldsymbol{q}_s$ [10,11]. Spacecraft and laboratory measurements as well as simulations have shown that energy fluxes are directed outward along the exhaust and that the ion enthalpy flux is typically the largest outflow component [10–17]. Space observations also show that outward-directed Poynting flux can be significant at the edges of the reconnection outflow at and near the separatrices [11,18–22].

High time resolution measurements from the Magnetospheric Multiscale (MMS) [23] mission offer a new opportunity to study this problem. Prior to MMS, spacecraft measurements were not able to resolve either the electron energy flux fine structure, or the vicinity of the electron dissipation region (EDR) in detail. MMS has revealed significant energy transfer processes are in fact occurring

in the EDR [24–28], indicating potentially significant differences in energy partition at the electron and ion scales.

Here, we use MMS data to show in new detail the nature of the energy flux densities in the vicinity of the EDR, and in the exhausts on either side. We examine the EDR encounter at 13:07:02.2 UT on 16 October 2015 [24,29]. This is an asymmetric reconnection event with a relatively weak out-of-plane (guide) magnetic field [30]. Although the overall ion energy flux density behavior is consistent with previous results, the ion heat flux density is reversed, directed toward the EDR. More surprisingly, there is a very significant out-of-plane electron energy flux density in the vicinity of the EDR whose magnitude is comparable to the ion energy flux density in the outflow. Conventional 2D models typically ignore this flux density because it does not contribute to the net energy flux into the diffusion region, but such models may be insufficient to capture magnetopause energy transport processes relating to particle acceleration, transport, and wave generation. This flux also suggests the possible existence of mesoscale and macroscale three-dimensional effects, even though the magnetopause reconnection geometry tends to be locally two dimensional.

Data and overview.—Figure 1 shows an overview of MMS4 magnetic (128 vector/s) and electric (8192 vector/s) field data [31–34], together with fast plasma instrument measurements of 3D electron (30 msec) and ion (150 msec) distributions [35]. We use a previously defined current sheet coordinate system [29] where $\boldsymbol{L}$ contains the reconnecting magnetic field and the reconnection exhausts, $\boldsymbol{M}$ is out of the reconnection plane, and $\boldsymbol{N}$ is normal to the current sheet directed out of the magnetosphere. Similar results are found for the other MMS spacecraft.

Initially MMS4 was in the magnetosheath ($B_L < 0$), and then crossed the magnetopause observing a $-v_{i,L}$ reconnection exhaust. At 13:06:58 UT n reduced, $|B|$ increased, and there was a significant increase in electric field fluctuations, suggestive of a separatrix region encounter on the magnetospheric exhaust edge. Enhanced fluctuations in $\boldsymbol{E}$ are then seen up to the EDR encounter at 13:07:02.2 UT. Enhanced $T_{e\|}$ is observed both in the vicinity of the separatrix and adjacent to the EDR. In contrast $T_{i,\perp} > T_{i,\|}$, except in the vicinity of the separatrix where T_i is enhanced and isotropic. At the EDR $\boldsymbol{v}_{i,\mathrm{LMN}} = (-137, -142, -3)$ km s^{-1} (averaged from 13:07:02.1 to 13:07:02.3 UT). For symmetric antiparallel reconnection, the stagnation point and the X line are colocated, whereas under more general boundary conditions they are not [36]. For this event it is expected that the stagnation point and X line are separated in the $\boldsymbol{N}$ direction, with the stagnation point being located toward the lower-density magnetosphere [37]. This is consistent with the observations where the reversal in B_L does not occur during the marked EDR encounter which is in the vicinity of the stagnation point, but immediately afterward (Sunward) [29]. A $+v_{\mathrm{i,L}}$ exhaust

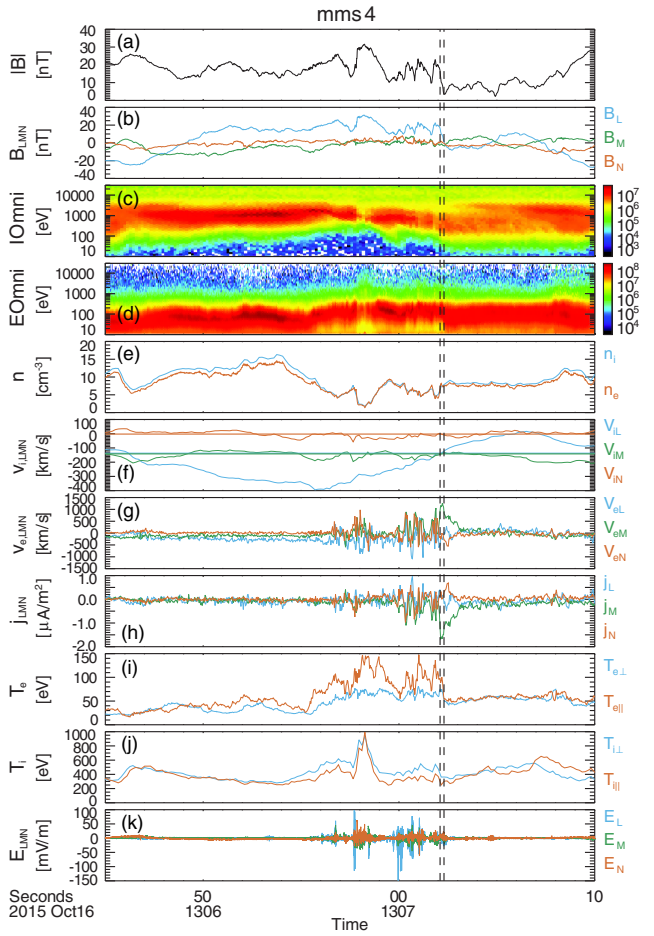

FIG. 1. (a),(b) magnetic field strength and components; (c),(d) ion and electron omnidirectional energy flux spectrograms; (e) ion and electron number density; (f),(g) ion and electron velocity (horizontal lines mark the ion velocity at the EDR); (h) current density derived from particle measurements; (i),(j) electron and ion parallel and perpendicular temperatures; (k) electric field. Vertical dashed lines mark a 0.2 s interval centered on the EDR encounter at 13:07:02.2 UT.

relative to the EDR was then observed, during which time MMS4 crossed back to the magnetospheric side ($B_L > 0$ at 13:07:05 UT) and finally into the magnetosheath ($B_L < 0$ after 13:07:07.5 UT).

Energy flux density calculations.—In understanding the energy partition in a quasisteady system, the relevant quantities are ultimately $\boldsymbol{Q}_s$ [8], which we construct via the standard decomposition approach which treats the underlying population as a single distribution. The kinetic energy flux density of species s is

$$\boldsymbol{K}_s = \frac{1}{2} n m_s v_s^2 \boldsymbol{v}_s,$$

where n is the number density, m_s is the particle mass, and $\boldsymbol{v}_s$ is the bulk velocity. To calculate this flux in the X-line frame (frame F), we transform the observations from the

spacecraft frame (F') using $\boldsymbol{v}_s^F = \mathbf{v}_s^{F'} - \boldsymbol{v}_{x\text{-line}}$ where $\boldsymbol{v}_{x\text{-line}}$ is taken to be the ion velocity at the EDR encounter since $v_i^F \approx 0$ in the EDR. The assumption of uniform steady X-line motion is considered reasonable, as over the 25 s interval shown in Fig. 1 the EDR moves only ~0.5 Earth radii in the $-\boldsymbol{L}$ direction relative to MMS, and MMS translates along the EDR in the $-\boldsymbol{M}$ direction by a similar amount. The enthalpy flux density of species s is

$$\boldsymbol{H}_s = \frac{\boldsymbol{v}_s \mathrm{Tr}(\overleftrightarrow{\boldsymbol{P}_S})}{2} + \boldsymbol{v}_s \cdot \overleftrightarrow{\boldsymbol{P}_s}$$

where $\boldsymbol{v}_s$ is transformed as described above, and $\overleftrightarrow{\boldsymbol{P}_s}$ is the pressure tensor [8]; this does not require the ratio of specific heats to be specified as was done in previous approaches [11]. The heat flux density, $\boldsymbol{q}_s$, is calculated directly from the fast plasma instrument data. Finally, the Poynting flux density is

$$\boldsymbol{S} = \frac{\boldsymbol{E} \times \boldsymbol{B}}{\mu_0} = \frac{(\boldsymbol{E}' + \boldsymbol{v}_{x\text{-line}} \times \boldsymbol{B}) \times \boldsymbol{B}}{\mu_0}$$

where $\boldsymbol{E}'$ is the electric field in the spacecraft frame and is averaged to the cadence of the magnetic field data.

In general, the ion energy flux densities are smoothly varying and the largest components are typically observed in the $\pm\boldsymbol{L}$ direction. $K_{i,L}$ [Fig. 2(d)] appears quite asymmetric because it scales as v_i^3 and the peak positive and negative ion exhaust speeds relative to the X line are approximately $+150\ \mathrm{km\,s^{-1}}$ and $-250\ \mathrm{km\,s^{-1}}$, respectively. $H_{i,L}$ [Fig. 2(e)] dominates and is the largest component on both sides of the EDR encounter. Unlike previous magnetotail observations [11] in this particular event $q_{i,L}$ is "backward" and directed toward the EDR on both sides. However, $\boldsymbol{Q}_i$ is directed away from the EDR in the $-\boldsymbol{L}$ direction prior to the EDR encounter, peaking at $-0.4\ \mathrm{mW\,m^{-2}}$. After the EDR encounter, $Q_{i,L}$ is positive, peaking at $\sim 0.2\ \mathrm{mW\,m^{-2}}$, but there is a comparable out-of-plane energy flux in the $-\boldsymbol{M}$ direction as well. The total ion energy flux densities are therefore approximately equal at 0.3–0.4 $\mathrm{mW\,m^{-2}}$.

In contrast to the ions, the electron energy flux densities are very structured and filamentary. Given the strong out-of-plane current density at the EDR, the distinct localized peak in $K_{e,M}$ [Fig. 2(i)] is to be anticipated; nevertheless, $\boldsymbol{K}_e$ makes a negligible contribution to the overall energy flux, as expected because it is proportional to m_e [11].

However, $\boldsymbol{H}_e$ [Fig. 2(j)] is surprisingly large in the $+\boldsymbol{M}$ direction near the EDR and is an order of magnitude bigger than $\boldsymbol{K}_e$. This corresponds to where both v_{eM} is large [Fig. 2(h)] and $T_{e\|}$ is elevated [Fig. 1(i)]. Its magnitude is comparable to the ion energy flux densities in the outflow and reveals significant out-of-plane electron energy transport at the EDR. $\boldsymbol{q}_e$ [Fig. 2(k)] is largely negligible; the

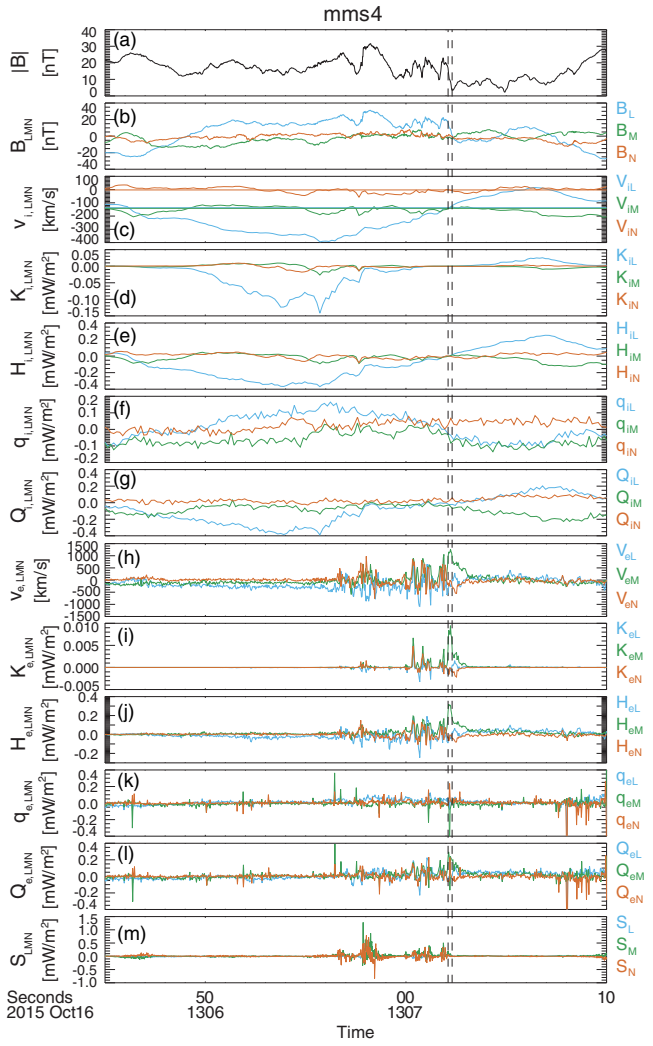

FIG. 2. (a),(b) magnetic field strength and components; (c) ion velocity in the spacecraft frame; (d)–(g) ion kinetic, enthalpy, heat, and total energy flux densities in the X-line frame; (h) electron velocity; (i)–(l) electron kinetic, enthalpy, heat, and total energy flux densities in the X-line frame; (m) Poynting flux density in the X-line frame.

negative peak in the EDR encounter is due to an artifact in one data point [38]. $\boldsymbol{Q}_e$ is thus dominated by H_{eM} which peaks in the EDR. This also reveals that the largest enhanced electron energy flux densities are closely associated with the stagnation point, and not the X line which is observed shortly afterward. Compared to $\boldsymbol{Q}_i$, $\boldsymbol{Q}_e$ is localized, but the peak magnitude in the EDR ~0.2–0.3 $\mathrm{mW\,m^{-2}}$ is comparable to the peak $\boldsymbol{Q}_i$ along the outflow.

The largest Poynting flux densities [Fig. 2(m)] are observed at ~13:06:58 UT, in the vicinity of the separatrix. $\boldsymbol{S}$ is ~0.75 $\mathrm{mW/m^2}$, with peaks above 1 $\mathrm{mW/m^2}$; significantly larger than either of the particle energy fluxes. There are then further intervals of enhanced $\boldsymbol{S}$ (at ~0.4 $\mathrm{mW/m^2}$) until the EDR encounter itself. The

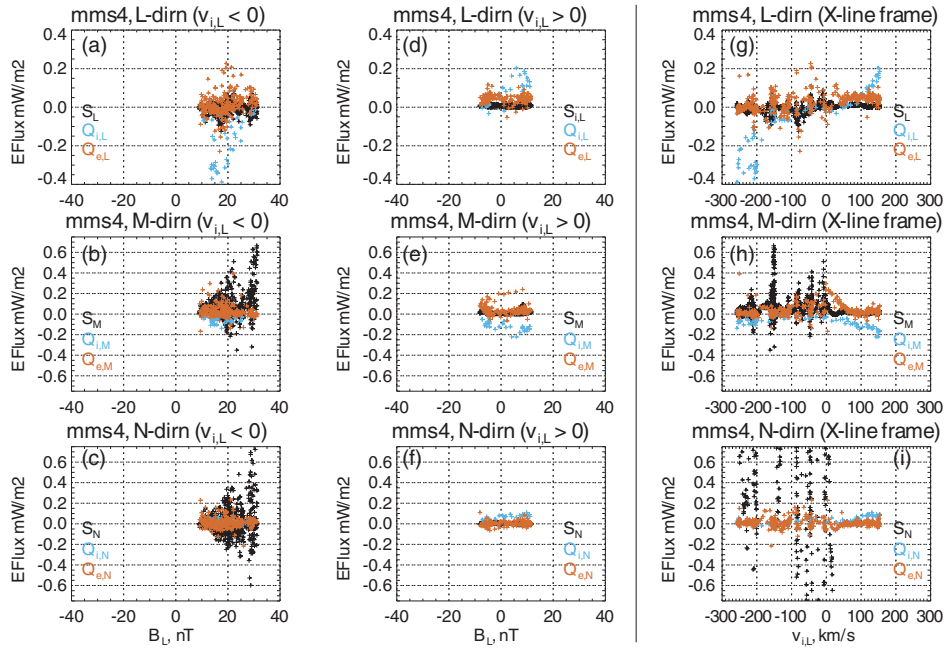

FIG. 3. (a)–(c) total ion energy flux, electron energy flux, and Poynting flux as a function of B_L for $v_{i,L} < 0$). (d)–(f) total ion energy flux, electron energy flux, and Poynting flux as a function of B_L for $v_{i,L} > 0$). (g)–(i) total ion energy flux, electron energy flux, and Poynting flux as a function of $v_{i,L}$. From top to bottom each row shows the L, M, and N components. All data are in the X-line frame.

intervals of strongest $\boldsymbol{S}$ do not necessarily correspond to the largest electric fields [cf. Fig. 1(k)], since $\boldsymbol{S}$ also depends on $\boldsymbol{B}$. In particular, $\boldsymbol{S}$ is relatively weak near the EDR, since $|B|$ is reduced in this region. Finally, $\boldsymbol{S}$ is negligible after the EDR encounter.

For context, variations in $\boldsymbol{Q}_i$ and $\boldsymbol{Q}_e$ and $\boldsymbol{S}$ are plotted together with the total energy density [8] of each species in the Supplemental Material [39]. Enhancements in U_e are structured, showing localized increases near the EDR and near the separatrix, whereas U_i varies more smoothly through the event.

In the absence of precise information about the location of MMS relative to the X-line, B_L and $v_{i,L}$ (in the X-line frame) can be used as proxies; the sign and size of B_L characterizes whether MMS is on the magnetospheric or magnetosheath side, and the distance to the magnetopause since $|B_L|$ increases with distance normal to the magnetopause. Figures 3(a)–3(c) show data as a function of B_L in the $-v_{i,L}$ exhaust, corresponding to the interval 13:06:54–13:07:02.2 UT. In the $\boldsymbol{L}$ direction $Q_{i,L}$ dominates, and is negative, appearing to peak on the $+B_L$ (magnetospheric) side. However, only a limited range of B_L is covered during the central flow reversal. In the $\boldsymbol{M}$ direction, $Q_{e,M}$ exceeds $Q_{i,M}$. There is a much stronger S_M component on the magnetospheric edge at the separatrix. In the $\boldsymbol{N}$ direction, the energy fluxes are dominated by fluctuating S_N. $\langle S_N \rangle$ is positive, and therefore directed into the exhaust from the magnetospheric side.

Figures 3(d)–3(f) show similar data as a function of B_L but in the $+v_{i,L}$ exhaust, corresponding to the interval 13:07:02.2–13:07:07 UT after the EDR encounter. In the $\boldsymbol{L}$ direction, $Q_{i,L}$ again dominates and peaks on the magnetospheric side. In the $\boldsymbol{M}$ direction, $Q_{e,M}$ is large and positive. The distribution of enhanced electron flux density over the region where $B_L > 0$ corresponds to the first part of this subinterval during the EDR, which shows that it is on the magnetospheric side of the X line, in the stagnation region, and not centered on the reversal in B_L. Finally, in the $\boldsymbol{N}$ direction there is little variation compared to the other components and times, but MMS did not encounter the separatrix on this side of the EDR.

The sign and size of $v_{i,L}$ in the X-line frame characterizes which exhaust MMS is located in and the distance from the X line along the outflow, since $v_{i,L}$ increases with downstream distance from the X line. Figures 3(g)–3(i) show data for the whole reversal (13:06:54–13:07:07 UT) as a function of $v_{i,L}$. In the $\boldsymbol{L}$ direction, $Q_{i,L}$ dominates, increasing with $v_{i,L}$ and distance from the X line. This is consistent with previous work and shows that there is a net ion energy flux away from the X line. $Q_{e,L}$ is highly structured with some suggestion of a similar divergence, however, the data must be interpreted with care, since on the $-v_{i,L}$ side, most of the data is from $B_L > 0$ near the separatrix. In the $\boldsymbol{M}$ direction $Q_{e,M}$ peaks around $v_{i,L} = 0$, consistent with the EDR encounter. Peaks in S_M and S_N at specific velocities arise because MMS crossed the separatrix at different distances from the X line (cf. Figs. 1 and 2) only detecting large $\boldsymbol{S}$ when at the appropriate B_L.

Discussion and conclusions.—Compared to previous observations, the ion energy flux densities are as expected,

being relatively smoothly varying, dominated by the L component, and increasing along the outflow with distance from the EDR. Unlike measurements in the symmetric magnetotail current sheet, the energy flux density is higher on the magnetospheric side [5]. One unusual feature of this event is that $\boldsymbol{q}_i$ is directed toward the EDR on both sides. However, in the equations governing energy transfer ultimately only the total energy flux density is relevant [8]. Decomposing the total energy flux density using a standard approach may give counterintuitive results if the underlying distribution is disjoint (consisting of beams) or is non-Maxwellian [40].

An unexpected feature of the data is that the electrons exhibit localized, structured energy fluxes which are dominated by an out-of-plane component in the vicinity of the EDR. This flux arises from the combination of the large out-of-plane electron velocity and the enhanced electron temperature. It is comparable in magnitude to the ion energy flux in the main exhaust, and indicates significant electron energy transport. In considering the energetics of reconnection, the existence of fast out-of-plane flow has been reported as a feature of symmetric reconnection configurations with no applied guide field in simulations, laboratory experiments, and in space [10,41–44]. Thus, although under asymmetric conditions the observed enhanced energy fluxes are at the stagnation point, under symmetric conditions, this is likely to be more significant at the X line since this is colocated with the stagnation point and EDR.

Finally, we note that $\boldsymbol{S}$ is not localized at the EDR but is associated with the separatrix region and directed into the exhaust. This is related to previous observations of strong electric fields in this region [18], and simulations indicating that electron-driven instabilities may also cause strong electrostatic turbulence and heating [45].

Previous observations have suggested that the smallest energy flux densities are encountered in the vicinity of the EDR [11], but here we have used the high-time resolution MMS measurements to show in new detail that large out-of-plane electron energy flux densities arise at the EDR, comparable in intensity to the ion energy fluxes in the main reconnection outflow. While these flux densities are more spatially localized than the larger-scale exhaust outflows, we suggest that they may significantly impact models of electron transport, wave generation, and particle acceleration.

If the magnetopause reconnection geometry were truly 2D, then out-of-plane fluxes are ignorable (in the sense that they would be invariant along the out-of-plane direction and would not contribute to the net energy transport). However, in real systems such as the magnetopause, this out-of-plane energy transport must eventually terminate or be diverted, and so the electron energy fluxes observed here may have corresponding large-scale 3D signatures on the magnetopause. There is therefore a need to explore more carefully the three dimensionality of reconnecting systems such as the magnetopause in light of the large out-of-plane flux densities reported here.

The MMS data used in this study are available from the MMS Science Data Center hosted by the Laboratory for Atmospheric and Space Physics (LASP) at the University of Colorado Boulder [46].

We acknowledge the support of UKRI/STFC (Grant No. ST/S000364/1 to J. P. E., J. E. S.), NASA (Grant 80NSSC18K0157 to T. D. P.; NNX17AI25G to M. A. S.; 80NSSC19M0146 to P. A. C.), DOE (Grant No. DE-SC0020294 to P. A. C.), and NSF (Grant No. PHY1804428 to P. A. C.), and thank the International Space Science Institute for its support and hospitality. Work at IRAP and LAB was supported by CNRS and CNES.

*jonathan.eastwood@imperial.ac.uk

[1] M. Yamada, Phys. Plasmas **14**, 058102 (2007).
[2] G. Paschmann, M. Øieroset, and T. Phan, Space Sci. Rev. **178**, 385 (2013).
[3] S. A. Fuselier and W. S. Lewis, Space Sci. Rev. **160**, 95 (2011).
[4] R. Blandford, Y. Yuan, M. Hoshino, and L. Sironi, Space Sci. Rev. **207**, 291 (2017).
[5] J. Birn, J. Borovsky, M. Hesse, and K. Schindler, Phys. Plasmas **17**, 052108 (2010).
[6] C. C. Haggerty, M. A. Shay, J. F. Drake, T. D. Phan, and C. T. McHugh, Geophys. Res. Lett. **42**, 9657 (2015).
[7] M. Hoshino, Astrophys. J. **868**, L18 (2018).
[8] M. V. Goldman, D. L. Newman, and G. Lapenta, Space Sci. Rev. **199**, 651 (2016).
[9] M. Yamada, J. Yoo, and C. E. Myers, Phys. Plasmas **23**, 055402 (2016).
[10] M. Yamada, J. Yoo, J. Jara-Almonte, H. Ji, R. M. Kulsrud, and C. E. Myers, Nat. Commun. **5**, 4774 (2014).
[11] J. P. Eastwood, T. D. Phan, J. F. Drake, M. A. Shay, A. L. Borg, B. Lavraud, and M. G. G. T. Taylor, Phys. Rev. Lett. **110**, 225001 (2013).
[12] E. Tyler, C. Cattell, S. Thaller, J. Wygant, C. Gurgiolo, M. Goldstein, and C. Mouikis, J. Geophys. Res. **121**, 11,798 (2016).
[13] M. Yamada *et al.*, Nat. Commun. **9**, 5223 (2018).
[14] M. Yamada, J. Yoo, J. Jara-Almonte, W. Daughton, H. Ji, R. M. Kulsrud, and C. E. Myers, Phys. Plasmas **22**, 056501 (2015).
[15] J. Yoo, B. Na, J. Jara-Almonte, M. Yamada, H. Ji, V. Roytershteyn, M. R. Argall, W. Fox, and L.-J. Chen, J. Geophys. Res. **122**, 9264 (2017).
[16] S. Lu, P. L. Pritchett, V. Angelopoulos, and A. V. Artemyev, Phys. Plasmas **25**, 012905 (2018).
[17] N. Aunai, G. Belmont, and R. Smets, Phys. Plasmas **18**, 122901 (2011).
[18] R. E. Ergun *et al.*, Phys. Rev. Lett. **116**, 235102 (2016).
[19] J. E. Stawarz *et al.*, Geophys. Res. Lett. **44**, 7106 (2017).

[20] M. A. Shay, J. F. Drake, J. P. Eastwood, and T. D. Phan, Phys. Rev. Lett. **107**, 065001 (2011).
[21] L. Price, M. Swisdak, J. F. Drake, J. L. Burch, P. A. Cassak, and R. E. Ergun, J. Geophys. Res. **122**, 11,086 (2017).
[22] L. Price, M. Swisdak, J. F. Drake, P. A. Cassak, J. T. Dahlin, and R. E. Ergun, Geophys. Res. Lett. **43**, 6020 (2016).
[23] J. L. Burch, T. E. Moore, R. B. Torbert, and B. L. Giles, Space Sci. Rev. **199**, 5 (2016).
[24] J. L. Burch *et al.*, Geophys. Res. Lett. **45**, 1237 (2018).
[25] M. Swisdak, J. F. Drake, L. Price, J. L. Burch, P. A. Cassak, and T.-D. Phan, Geophys. Res. Lett. **45**, 5260 (2018).
[26] K. J. Genestreti *et al.*, J. Geophys. Res. **122**, 11,342 (2017).
[27] K. J. Genestreti, P. A. Cassak, A. Varsani, J. L. Burch, R. Nakamura, and S. Wang, Geophys. Res. Lett. **45**, 2886 (2018).
[28] S. Wang, L.-J. Chen, N. Bessho, M. Hesse, J. Yoo, M. Yamada, Y.-H. Liu, D. J. Gershman, B. L. Giles, and T. E. Moore, J. Geophys. Res. **123**, 8185 (2018).
[29] J. L. Burch *et al.*, Science **352**, aaf2939 (2016).
[30] R. E. Denton, B. U. Ö. Sonnerup, H. Hasegawa, T. D. Phan, C. T. Russell, R. J. Strangeway, B. L. Giles, D. Gershman, and R. B. Torbert, Geophys. Res. Lett. **43**, 5589 (2016).
[31] C. T. Russell *et al.*, Space Sci. Rev. **199**, 189 (2016).
[32] R. E. Ergun *et al.*, Space Sci. Rev. **199**, 167 (2016).
[33] P.-A. Lindqvist *et al.*, Space Sci. Rev. **199**, 137 (2016).
[34] R. B. Torbert *et al.*, Space Sci. Rev. **199**, 105 (2016).
[35] C. Pollock *et al.*, Space Sci. Rev. **199**, 331 (2016).
[36] J. P. Eastwood, T. D. Phan, M. Oieroset, M. A. Shay, K. Malakit, M. Swisdak, J. F. Drake, and A. Masters, Plasma Phys. Controlled Fusion **55**, 124001 (2013).
[37] P. A. Cassak and M. A. Shay, Phys. Plasmas **14**, 102114 (2007).
[38] A. C. Barrie, S. E. Smith, J. C. Dorelli, D. J. Gershman, P. Yeh, C. Schiff, and L. A. Avanov, J. Geophys. Res. **122**, 765 (2017).
[39] See Supplemental Material at http://link.aps.org/supplemental/10.1103/PhysRevLett.125.265102 for further information about the behavior of total energy densities during this event.
[40] M. V. Goldman, D. Newman, J. P. Eastwood, and G. Lapenta, J. Geophys. Res. **125**, e2020JA028340 (2020).
[41] M. E. Mandt, R. E. Denton, and J. F. Drake, Geophys. Res. Lett. **21**, 73 (1994).
[42] M. A. Shay, J. F. Drake, R. E. Denton, and D. Biskamp, J. Geophys. Res. **103**, 9165 (1998).
[43] T. Nagai, I. Shinohara, M. Fujimoto, A. Matsuoka, Y. Saito, and T. Mukai, J. Geophys. Res. **116**, A04222 (2011).
[44] R. B. Torbert *et al.*, Science **362**, 1391 (2018).
[45] M. Hesse *et al.*, Phys. Plasmas **25**, 122902 (2018).
[46] J. L. Burch *et al.*, MMS Science Data Center, 2020,https://lasp.colorado.edu/mms/sdc/public/.